Optical Engineering

SPIEDigitalLibrary.org/oe

Application of digital speckle interferometry to visualize surface changes in metallic samples immersed in $Cu(NO_3)_2$ solutions

Nieves Andrés
Ana Andres-Arroyo
M. Pilar Arroyo
Virginia R. Palero
Julia Lobera
Luis A. Angurel

Application of digital speckle interferometry to visualize surface changes in metallic samples immersed in $Cu(NO_3)_2$ solutions

Nieves Andrés
Ana Andres-Arroyo
M. Pilar Arroyo
Virginia R. Palero
Universidad de Zaragoza
Instituto de Investigación en Ingeniería de Aragón
Facultad de Ciencias, c/Pedro Cerbuna 12
Zaragoza 50009, Spain
E-mail: nandres@unizar.es

Julia Lobera
Centro Universitario de la Defensa de Zaragoza
Carretera Huesca S/N, Zaragoza 50090, Spain

Luis A. Angurel
Instituto de Ciencia de Materiales de Aragón
(CSIC-Universidad de Zaragoza)
c/María de Luna 3, Zaragoza 50018, Spain

Abstract. Digital speckle pattern interferometry (DSPI) has been applied to analyze surface corrosion processes in a metallic sample immersed in a 0.1 M $Cu(NO_3)_2$ solution. The corrosion process induces changes in the surface and in the solution refractive index. A detailed analysis of the DSPI measurements has been performed to obtain a two-dimensional visualization of the surface changes and an evaluation of the refractive index changes of the solution. The possibilities of DSPI for measuring surface changes in these conditions have been analyzed. [DOI: 10.1117/1.OE.52.10.101918]

Subject terms: speckle interferometry; metrology; surface measurements; nondestructive testing.

Paper 130199SSP received Feb. 5, 2013; revised manuscript received Jul. 4, 2013; accepted for publication Jul. 10, 2013; published online Aug. 12, 2013.

1 Introduction

For engineering purposes, it is very important to know the durability of a material in some environments. When a metallic sample is immersed in some solutions, chemical reactions take place and the surface is altered or even destroyed. Traditional methods used to analyze corrosion processes that provide a global value for the sample, and it is usually measured after a long period of time. The early detection of these effects for preventive purposes is very interesting. Besides, as surface modifications take place locally and nonuniformly, the knowledge of how and where the processes start in different conditions is very valuable. These facts justify the development of experimental methods that could both accurately measure local corrosion rates and localize the corroding sites.

Optical techniques, due to their nondestructive character, have been applied to measure *in situ* changes in surfaces[1–14] as an alternative to traditional intrusive methods. Holographic techniques provide information about the evolution of the corrosion process in an aqueous solution by counting the number of fringes[3–5] or by monitoring the refractive index change in electrochemical reactions using an in-line recording setup.[6–11]

Digital speckle techniques are very useful for detecting surface modifications in solids.[15,16] Digital speckle photography has been applied to measure the local surface changes in corrosion processes and to estimate the corrosion rate.[12,13] Speckle interferometry, using a twin-object-beam recording system, has been applied to the study of corrosion to obtain a global value of the corrosion rate.[14] Digital speckle pattern interferometry (DSPI) has been employed to measure the thickness of the corrosion layer in a metallic surface but the sample had to be removed from the corrosion media before recording each image.[17]

As in many cases corrosion processes take place when the metallic surface is immersed in liquids, the possibility of measuring changes in the surface during the dynamic process would be very useful. For measurements inside liquids, concentration gradients, liquid movements, or changes in the refractive index can have a very important influence on the optical results limiting the applicability of the technique in these conditions.

In this work, changes that take place in a metallic surface while immersed in a $Cu(NO_3)_2$ solution have been investigated using DSPI. Two different contributions to the local speckle changes have been observed: modifications in the metallic surface and changes in the refractive index. Both contributions have been identified and separated. DSPI has been used to obtain two-dimensional (2-D) quantitative information about the evolution of the corrosion layer thickness. The limitations of DSPI as a 2-D characterization technique in the analysis of corrosion processes have been pointed out. Another important advantage of this technique is the recording of the temporal evolution, which makes possible to compare with the initial state or between different situations.

2 Digital Speckle Pattern Interferometry

DSPI is a well-known technique that records the interference of the light scattered by the object and a reference beam.[15,16] For this application, the object rough surface (speckle wave) is imaged onto the charge-coupled device (CCD) camera and the reference beam is a smooth laser beam. Both beams are obtained by splitting the main laser beam and are combined

by means of a beam-splitter cube placed in front of the CCD sensor. The interference pattern, known as specklegram, is recorded at different time instants, at least twice, before and after having slightly deformed or displaced the object.

In order to obtain quantitative information, phase shifting techniques must be introduced. These techniques are based on the addition of a known phase shift that can be introduced along the time in several recordings (Temporal Phase Shifting)[18] or in the same recording along a direction over the sensor [Spatial phase shifting (SPS)].[19] For dynamic processes, as corrosion ones, SPS techniques are suited.

Spatial phase shifting (SPS) techniques are used in our case to obtain a quantitative phase map (random) of the object scattered light. A conventional DSPI setup can be turned into a SPS-DSPI setup by shifting the origin of the divergent reference wave with respect to the lens center by a certain amount Δx and Δy, but keeping the same Z coordinate. X and Y coordinates define the surface plane and the Z axis the out-of-plane direction. This generates a linear phase shift over the sensor in a direction fixed by the x and y change. It produces phase-shifted data, which are recorded simultaneously on adjacent pixels, in the same speckle. Thus, to resolve this modulation frequency, a phase shift of 2π is recorded on each speckle. This requires increasing the speckle size up to about 3 pixels, which means a decrease in the spatial resolution.

The object phase map can be retrieved from each specklegram using a global Fourier transform method.[20,21] Two images of the object wave in the aperture plane (real and virtual image) appear on the Fourier plane and their position is related to the carrier frequency introduced by the shifting. One image is selected and translated to the origin to eliminate the frequency shift. Finally, its inverse Fourier transform is calculated, and the phase at each pixel is obtained from the real and imaginary parts of the complex amplitude distribution.

A phase difference map is calculated by subtracting two object phase maps obtained at different time instants. For visualization, these phase difference maps are mapped to gray levels being dark for $-\pi$ and bright for π. The calculated phase difference values lie in the range of 2π and values outside this range are wrapped. An unwrapping process, in which the phase is extended to a continuous range of more than 2π, is required for determining the deformation.

Phase differences, $\Delta\phi(x,y)$, are directly related to optical path length changes, $\Delta\delta(x,y)$. The origins of these $\Delta\delta(x,y)$ are local surfaces changes, $\mathbf{L}(x,y)$, and refractive index changes, $\Delta n(x,y)$ in the beam path.

Considering only surface displacements, the phase difference can be expressed as $\Delta\phi_L(x,y) = \mathbf{K}\cdot\mathbf{L}(x,y)$, where $\mathbf{L}(x,y)$ is the surface local displacement vector between the two states and $\mathbf{K} = (\mathbf{k}_o - \mathbf{k}_i)$ is the sensitivity vector, $\mathbf{k}_i$ and $\mathbf{k}_o$ being the wave vectors of the illumination and observation beams. The beams form an angle with the normal object surface vector of θ_i and θ_o, respectively. The modulus of these vectors is the same, $k = 2\pi n/\lambda_o$, where n is the refractive index and λ_o is the wavelength in the air. We will refer to the vector directions as $\mathbf{u}_i$ and $\mathbf{u}_o$, respectively. Thus, $\Delta\phi_L(x,y)$ can be expressed as:

$$\Delta\phi_L(x,y) = \frac{2\pi}{\lambda_o} n(\vec{u}_o - \vec{u}_i)\cdot\vec{L} = \frac{2\pi}{\lambda_o} n|\vec{u}_o - \vec{u}_i|L_K, \qquad (1)$$

where L_K is the projection of the surface displacement along the direction of the sensitivity vector. In our case, L_K is expected to be very small and, in these conditions, n is the value of the refractive index close to the sample surface.

Corrosion surface changes produce a modification of the corrosion layer thickness. These changes are expected to produce the same effect than displacements in the out-of-plane direction. Considering Cartesian coordinates and the previously defined axes, the components of the sensitivity vector in the Y direction can be neglected, $k_{iy} = 0$ and $k_{oy} = 0$. Thus, the phase change in corrosion processes is related with surface displacements by the following equation:

$$\Delta\phi_L(x,y) = \frac{2\pi}{\lambda_o} n(x,y)[L_z(x,y)(\cos\theta_i + \cos\theta_o)], \qquad (2)$$

where $L_z(x,y)$ should reflect the evolution of the corrosion layer thickness in each point of the surface.

When the object is immersed in a liquid solution, the local chemical modifications in the solution, which are related to the corrosion activity, can produce changes in the refractive index along the beam. They also contribute to the total phase change. Considering only refractive index changes, the phase differences can be expressed as:

$$\Delta\phi_n(x,y,z) = \frac{2\pi}{\lambda_o}\Delta\delta(x,y,z) = \frac{2\pi}{\lambda_o}\int_0^d \Delta n(x,y,z)\mathrm{d}l, \qquad (3)$$

where l refers to positions along the beam travelling path and d is the total length with refractive index changes.

For DSPI experiments carried out while the surface is immersed in a corrosive solution, the measured phase change is due to both contributions, i.e., $\Delta\phi(x,y) = \Delta\phi_L(x,y) + \Delta\phi_n(x,y)$. Although the corrosion process is the origin of both changes, we are interested in obtaining $\Delta\phi_L(x,y)$ from the measurement of $\Delta\phi(x,y)$ because it determines the evolution of the corrosion layer.

In order to study the dynamic evolution, series of images are sequentially recorded while changes are taking place. The comparison can be done with the reference initial state, recorded before any modification has been produced, or between different surface states. Due to the nature of interferometric techniques, each phase map is random and presents an unknown global phase change. In order to be able to compare images recorded at different time instants, a reference phase value in a given region of the sample is required.

3 Experimental Setup

The optical experimental setup is shown in Fig. 1. A He-Ne laser ($\lambda = 633$ nm) of 17 mW is split in two beams by means of a wedge. The reference laser beam is guided by an optical fiber. The sample is illuminated with a collimated laser beam, under an angle of 20 deg and imaged onto a CCD camera by a 60 mm focal length lens with a magnification of 0.53. Both beams are combined using a beam splitter cube placed in front of the CCD camera. The CCD sensor has 1376 (vertical) × 1040 pixels with a size of 6.4 μm/pixel. The images have 4096 gray levels. With these experimental conditions, the object length recorded in the vertical direction is 12.5 mm with a spatial resolution of 12 μm. Series of images with an exposure time of 5 ms were recorded every 2 s during 2000 s. A rectangular iron sample

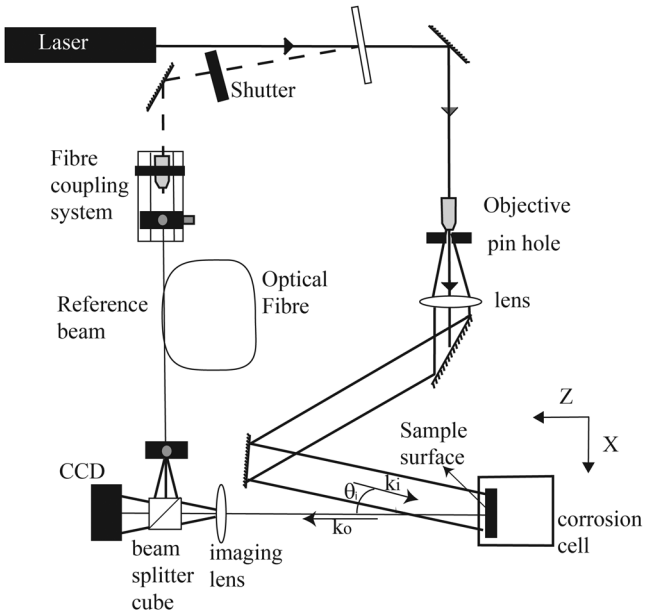

Fig. 1 Optical setup for a digital speckle pattern interferometry (DSPI) with spatial phase shifting (SPS).

(5 mm wide) has been used in the experiments. The sample is held on a solid structure fixed to the optical table to avoid global movements. It is placed parallel to the CCD sensor in order to focus the whole surface. The sample is partially immersed in a corrosion cell filled with 0.1 M of $Cu(NO_3)_2$ to have a noncorroded area that could be used as a reference for the phase. The object surface is located close to the cell front wall, 6 mm away in our case, to reduce the influence of the liquid refractive index change in the speckle pattern. Between the upper part of the sample and the immersed area, there is a dark region, which corresponds to the shadows from the cell edge and from the liquid upper surface. Thus, the length of the visualized immersed iron sample is 6.6 mm.

During the corrosion process, copper atoms are deposited over the iron surface, and iron atoms move to the solution. These modifications produce a change in the solution composition and in the corrosion layer over the sample surface.

In the setup used in this work, with recording angles of $\theta_i = 20$ deg and $\theta_o = 0$ deg and considering only surface changes, information related to the out-of-plane displacement is retrieved, which is the most important in corrosion processes. According to Eq. (2), the displacement $L_z(x, y)$, which corresponds to the evolution of the corrosion layer thickness, L_c, is measured as:

$$L_c(x, y) = \frac{\Delta\phi_L(x, y)}{2\pi} \frac{\lambda_o}{n(\cos\theta_i + \cos\theta_o)}. \quad (4)$$

It corresponds to about 0.24 μm/fringes, being $n = 1.34$ the refractive index of the $Cu(NO_3)_2$, as measured with an Abbe refractometer.

To visualize the changes in the liquid refractive index, an aluminum sample that is not affected by this corrosive solution is placed next to the iron sample. Taking into account that the total length of the beam inside the liquid is $d = 12$ mm and Eq. (3), the change in the refractive index that can be visualized with our geometry corresponds to about 5.2×10^{-15} per fringe.

4 DSPI Analysis

The first step in the analysis process is to calculate the wrapped phase difference map [Fig. 2(a)]. For visualization, these phase differences maps are presented using gray levels being $-\pi$ for dark values and π for bright values. As the maximum accuracy established for this technique is around a fringe/100, 256 gray levels have been used for the visualization.

As it can be seen in Fig. 2(a), there is no information from the surface changes in some areas. To improve the visualization, the images have been divided in at least two areas: the immersed part and the one outside the liquid. Thus, a mask with a gray value of one in the object areas and zero in the rest of the image was used. The multiplication by this mask assures that the no interest areas are presented in black.

Due to the speckle appearance, filtering the image is needed for extracting the phase data at each point. Each

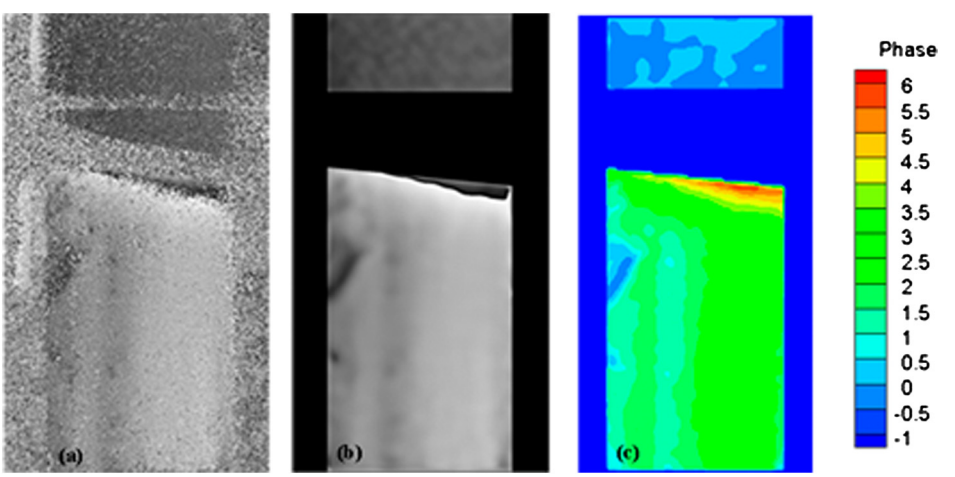

Fig. 2 (a) Phase map obtained by comparing the corrosion state after 180 s with the initial state. (b) Filtered map multiplied by the mask in order to eliminate the regions that are affected by the liquid and the corrosion cell edges. (c) Two-dimensional (2-D) surface phase map.

mask area can be filtered independently. A Window Fourier Transform filter[22] has been applied to the exponential field $f(x,y) = \exp[(j\Delta\phi(x,y)]$. The filtered phase map [Fig. 2(b)] is obtained from the real and imaginary parts of the filtered exponential field. The correct wrapped phase maps should have a null value in the sample noncorroded (upper) area. Thus, the filtered phase data for each image have been corrected by subtracting the measured phase in the corresponding noncorroded area.

The next step in the DSPI analysis is the phase unwrapping process to detect the 2π phase jumps for converting the phase into a continuous function. From the absolute phase data at each point, the 2-D surface changes can be visualized as isoline maps [Fig. 2(c)].

We have used both spatial and temporal phase unwrapping.[23,24] The spatial unwrapping is carried out by comparing the phase at neighboring pixels and adding the multiples of 2π to obtain the absolute phase. The temporal unwrapping detects the jumps by comparing the phase along the time and adding the 2π changes to the final phase.

The spatial unwrapping is useful in the comparison of any object surface state with the initial one. However, in our corrosion process, due to the discontinuity produced by the liquid layer, the absolute fringe order for the immersed surface cannot be easily determined from spatially unwrapped phase maps. On the other hand, the temporal unwrapping is useful for knowing the phase evolution at any point.

The absolute phase map at any time can be obtained either from the comparison with the initial state, using the temporal evolution only to detect the 2π phase jumps, or by adding the phase changes obtained at short time intervals. In our corrosion process, as the copper is deposited over the sample, the microstructure at these locations changes and produces speckle decorrelation. As is well known, no information can be obtained from these areas. Since the speckle decorrelation will be bigger when comparing with the initial state, the final phase has been obtained by adding the phase changes at short time intervals.

The accuracy in the phase retrieved from any phase map is determined by SPS technique and is established to be a fringe/100. When the final phase is calculated by adding several phase values, the final accuracy is expected to be lower. In our case, the final phase has been obtained by adding the phase changes corresponding to 10-s time intervals. To check the accuracy of this adding process, the phase at a time t obtained in the nonimmersed part of the sample with both methods has been compared. The data rms has been measured to be about twice bigger for the summing process when adding 50 phase maps ($t = 500$ s). This implies an error of 6-nm error in the displacement or 0.15 rad in the phase. The phase temporal evolution of selected points from the immersed area as calculated from a single phase map and from the adding process has been compared. Up to a maximum measured phase of 20 rad, the difference between both measurements is <3% with a lower limit of 0.15 rad.

The resolution of the unfiltered data depends on the magnification used in the setup, which was 12 μm/pixel. After the filtering process, which used a 10-pixel halfwidth Gaussian window, the final spatial resolution is estimated to be $\sim$100 μm.

5 Evaluation of the Refractive Index Changes

In these experiments, corrosion takes place both in the front and in the rear sample surfaces. During this process, an exchange of Cu and Fe ions between the sample and the liquid takes place leading to possible refractive index changes. As has been mentioned in Sec. 3, in order to be able to visualize the evolution of this contribution, an aluminum sample was placed next to the iron sample. As the aluminum is not affected by this corrosion process, any fringe observed over its surface is due to liquid refractive index changes originated on the Fe sample corrosion process. Thus, the analysis of the phase maps evolution (Fig. 3) allows to visualize the liquid refractive index change and how it propagates. Some fringes were originated in the upper right immersed corner of the Fe sample. From their evolution, it can be deduced that they correspond to changes in the refractive index and can be clearly seen after 120 s [Fig. 3(a)]. The number of fringes increases with time and the fringes propagate over the total area as the refractive index changes propagate. After 300 s, the index changes reach the aluminum sample area. Let us remark that in these experimental conditions, this process always starts in the upper part, close to the liquid surface. After 480 s, three fringes are observed and they correspond to a variation of refractive index of 1.5×10^{-4}.

From the 2-D phase maps, the path length changes in each point can be calculated. Figure 4 shows the 2-D maps for the path length change ($\delta = nL$) obtained from the phase maps presented in Fig. 3, whose main contribution in the immersed area close to the liquid surface is due to the refractive index changes. The number of fringes increases with time, even reaching the bottom and covering the whole surface image, which hides any information about the corrosion layer over the surface.

In order to confirm that these changes are due to variations in the solution refractive index, a typical Mach-Zehnder interferometer configuration has been used. In

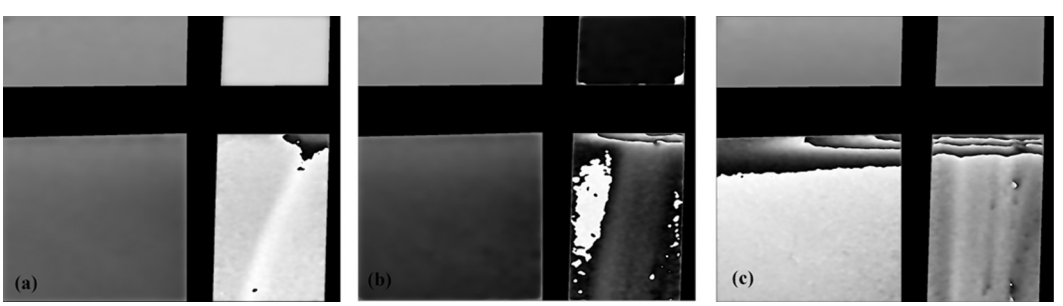

Fig. 3 Filtered phase maps obtained after a time of: (a) 120 s (b) 240 s, (c) 480 s. In all the cases, the reference was the initial state.

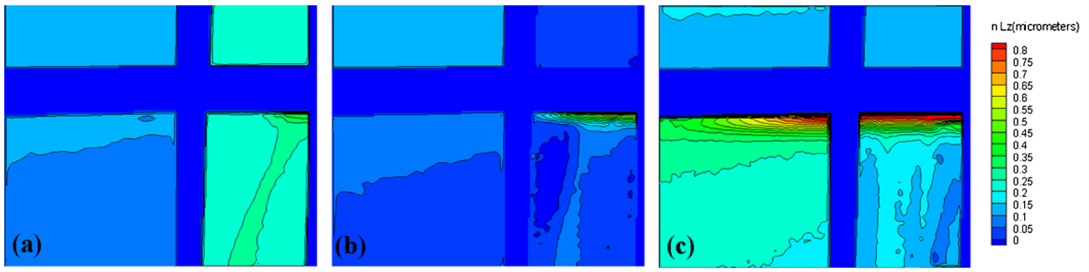

Fig. 4 Two-dimensional maps of the path length changes, δ, obtained after a time of: (a) 120 s, (b) 240 s, and (c) 480 s.

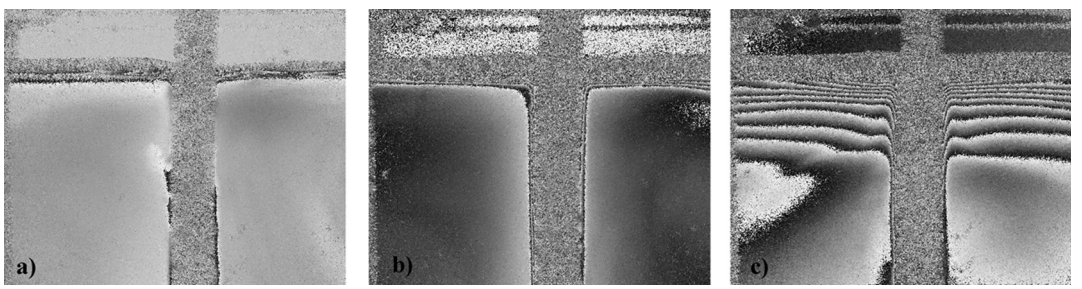

Fig. 5 Phase map obtained from a Mach–Zehnder setup at (a) 50 s, (b) 100 s, and (c) 2000 s.

this case, the illumination goes through a ground glass to produce a speckle wave. It travels across the liquid in front of the corroding surface that has been rotated. The phase change on the camera corresponds to changes in the speckle wave produced by the refractive index changes along the path. The phase maps obtained at different times after having initiated the corrosion process are shown in Fig. 5. In agreement with the results presented in Figs. 3 and 4, it is observed that the refractive index changes originate close to the sample and close to the liquid surface. In this case, the integration length corresponds to the width of the sample, which is ~5 mm.

6 Analysis of the Corrosion Process

Results presented in the previous section confirm that the changes in the refractive index are predominant in the upper part of the DSPI images, in the region close to the liquid surface. In consequence, information about the evolution of the corrosion layer can only be retrieved in the lower part of the sample. Although the corrosion process was recorded during 2000 s, the refractive index change in the lower part of the sample is only negligible for the first 500 s. After this time, the index variation covers the full sample, which prevents any information on the surface corrosion process from being obtained.

Figure 6 shows the lowest 5 mm of the iron sample at $t = 300$ s [Fig. 6(a)] and at $t = 480$ s [Fig. 6(b)]. The reference has been taken at $t = 0$ s and, in consequence, the corrosion layer at any position of the surface from the beginning of the process can be derived. Surface changes up to 200 nm have been measured. This corresponds to the left part of the images. In case of Fig. 6(b), a positive variation is measured in the right part of the images. This shows how the contribution of the refractive index variations starts to modify the DSPI surface observations.

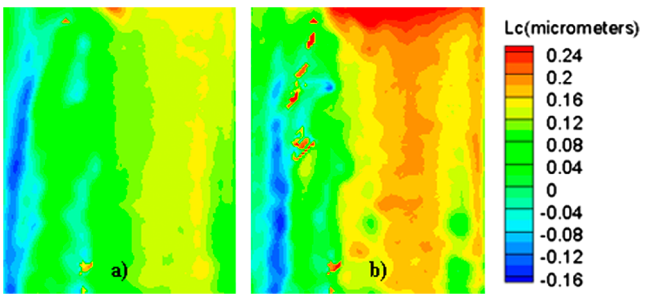

Fig. 6 Details of the corrosion layer on the Fe area which is not affected by liquid changes after (a) 300 s and (b) 480 s.

New experiments have been performed in a second sample. To minimize the contribution due to the refractive index changes over the sample image, it has been immersed in the solution only for 600 s and only the lowest part of the sample, far from the liquid edge, has been visualized. In this case, the opposite side and the borders of the observation side are covered with nail polish. These regions have been used as a reference region for the phase because in this case there is no access to a nonimmersed region of the sample. The corrosion takes place only in a region 2.3 mm wide and 15 mm long as presented in Fig. 7. In order to avoid the effects related to the refractive index changes produced on the liquid surface, only

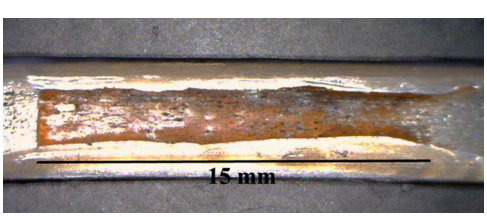

Fig. 7 Aspect of the corrosion region after 600 s.

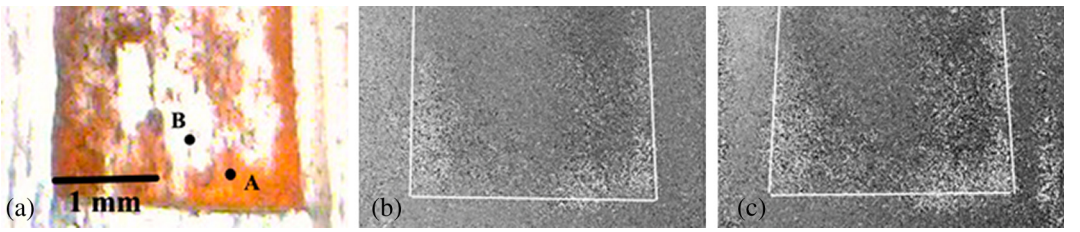

Fig. 8 (a) Detail of the lowest part of the corroded area. Phase difference maps recorded at 200 s (b) and 350 s (c).

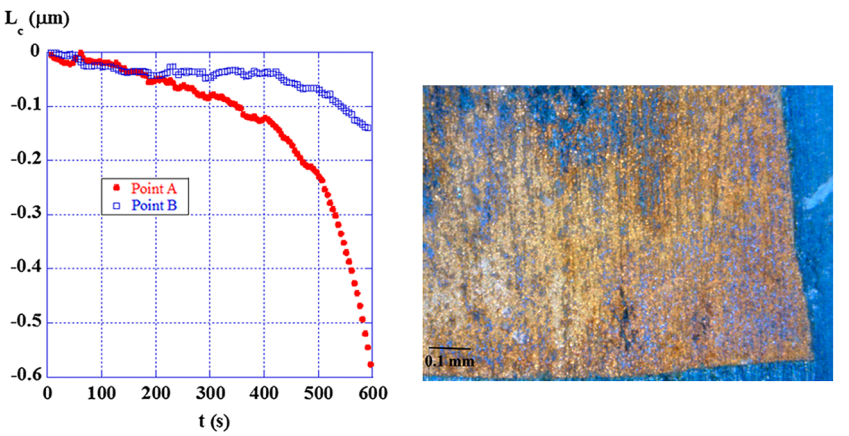

Fig. 9 (a) Evolution of the corrosion layer at the points A and B shown in Fig. 8(a). (b) Detail of the corrosion layer in the right corner.

the region in the lower 2 mm of the corroded area has been recorded.

Figure 8 shows a detail of the lowest part of the corroded area [Fig. 8(a)] and the phase difference maps observed in this region after 200 s [Fig. 8(b)] and 350 s [Fig. 8(c)]. The lighter regions in the phase difference maps correspond to the regions where the corrosion is taking place. As can be observed from the comparison with the photograph of the final sample surface, DSPI observations clearly detect where corrosion is most important. From the analysis on these images, it is possible to derive how the corrosion layer has evolved at each point of the sample. An example is presented in Fig. 9(a), where this evolution is presented for the points A and B shown in Fig. 8(a). The final corrosion depth is measured to be ~100 nm for point B and 600 nm for point A. The final phase difference map has been obtained by adding the phase changes measured every 5 s. It is possible to derive the ratio between the corrosion rates in both points, being near four times faster in point A than in point B, but it is more difficult to derive the exact value. As can be observed in detail of the corroded area [Fig. 9(b)], the corrosion layer is not uniform; small regions of Cu can be seen over the Fe surface.

7 Conclusions

DSPI has been presented as a technique to analyze the corrosion process of a metallic surface immersed in a corrosive liquid. Due to the nature of the corrosion process, the final thickness has been calculated by adding the thickness changes obtained every few seconds. Corrosion layer thicknesses of hundreds of nanometers with an accuracy of 3% (with lower limit of 6 nm) and a spatial resolution of 100 μm have been measured.

One of the main limitations of the technique is the solution composition changes which can be produced by the corrosion process. This leads to local refractive index changes, which contribute to the measured phase, masking the information related to the corrosion layer thickness. In consequence, a quantitative evaluation of the corrosion layer thickness evolution is only possible when changes in the refractive index are negligible.

Acknowledgments

Funding of this research by Spanish MINECO and the European FEDER Program (Project MAT2011-22719) and by Gobierno de Aragón (Research groups T12 and T76) is gratefully acknowledged. Authors would also like to acknowledge the use of Servicio General de Apoyo a la Investigación-SAI, Universidad de Zaragoza.

References

1. P.S. Huang, F. Jin, and F. Chiang, "Quantitative evaluation of corrosion by a digital fringe projection technique," *Opt. Lasers Eng.* **31**(5), 371–380 (1999).
2. J.P. Ying et al., "Nondestructive evaluation of incipient corrosion in a metal beneath paint by second-harmonic tomography," *Opt. Lett.* **25**(16), 1189–1191 (2000).
3. K. Habib and F. Al-Sabati, "Interferometric sensor for electrochemical studies of metalic alloys in aqueous solution," *Opt. Rev.* **4**(2), 324–328 (1997).
4. K. Habib, "In situ measurements of oxide film growth on aluminium samples by holographic interferometry," *Corros. Sci.* **43**(3), 449–455 (2001).
5. K. Habib, K. Al-Muhana, and A. Habib, "Holographic interferometry as electrochemical emission spectroscopy of carbon steel in seawater with low concentration of RA-41 corrosion inhibitor," *Opt. Laser Eng.* **46**(2), 149–156 (2008).
6. X. Yang et al., "In-line digital holography for the study of dynamic processes of electrochemical reaction," *Electrochem. Commun.* **6**(7), 643–647 (2004).

7. C. Wang et al., "Investigation of chloride-induced pitting processes of iron in the H2SO4 solution by the digital holography," *Electrochem. Commun.* **6**(10), 1009–1015 (2004).
8. B. Yuan et al., "Real time observation of the anodic dissolution of copper in NaCl solution with the digital holography," *Electrochem. Commun.* **11**(7), 1373–1376 (2009).
9. L. Li et al., "Numerical reconstruction of digital holograms for the study of pitting dynamic processes of the X70 carbon steel in NaCl solution," *Electrochem. Commun.* **10**(1), 103–107 (2008).
10. B. Yuan et al., "Investigation of the effects of the magnetic field on the anodic dissolution of copper in NaCl solutions with holography," *Corros. Sci.* **58**, 69–78 (2012).
11. B. Yuan et al., "Dynamic observation of the diffusion layer in anodic processes of the Fe/H2SO4 system with digital holography," *Electrochem. Commun.* **27**, 116–119 (2013).
12. N. Andrés et al., "Fast visualization of corrosion process using digital speckle photography," *Corros. Sci.* **50**(10), 2965–2971 (2008).
13. S. Recuero et al., "Visualization of environmental degradation in ceramic superconductors using digital speckle photography," *J. Eur. Ceram. Soc.* **28**(11), 2239–2246 (2008).
14. Y. Gao, Y. Ou, and M. Chen, "Measurements of the off-plane displacement of carbon steel corrosion with twin-object-beam electronic speckle interferometry," *Optik* **121**(19), 1756–1760 (2010).
15. P. K. Rastogi, *Digital Speckle-Pattern Interferometry and Related Techniques*, Wiley, Chichester, UK (2001).
16. C. M. Vest, *Holographic Interferometry*, Wiley, New York (1979).
17. N. Andrés et al., "Two-dimensional quantification of the corrosion process in metal surfaces using digital speckle pattern interferometry," *Appl. Opt.* **50**(10), 1323–1328 (2011).
18. K. Creath, "Temporal phase measurement methods," in *Interferogram Analysis*, D. W. Robinson and G. T. Reid, Eds., p. 94, Institute of Physics Publishing, Bristol (1993).
19. J. Burke et al., "Speckle intensity and phase gradients: influence on fringe quality in spatial phase shifting ESPI-systems," *Opt. Commun.* **152**(1–3), 144–152 (1998).
20. M. Takeda, H. Ina, and S. Kobayashi, "Fourier-transform method of fringe-pattern analysis for computer based topography and interferometry," *J. Opt. Soc. Am.* **72**(1), 156–160 (1982).
21. J. Lobera, N. Andrés, and M.P. Arroyo, "Digital speckle pattern interferometry as a holographic velocimetry technique," *Meas. Sci. Technol.* **15**(4), 718–724 (2004).
22. K. Qian, "Windowed Fourier transform for fringe pattern analysis," *Appl. Opt.* **43**(13), 2695–2702 (2004).
23. H.O. Saldner and J.M. Huntley, "Temporal phase unwrapping: application to surface profiling of discontinuous objects," *Appl. Opt.* **36**(13), 2770–2775 (1997).
24. J. M. Huntley, "Automated analysis of speckle interferogram," in *Digital Speckle Pattern Interferometry and Related Techniques*, P. K. Rastogi, Ed., pp. 59–140, John Willey and Sons, Chichester, England (2001).

Nieves Andrés has been associate professor of applied physics at the University of Zaragoza since 2001. Her main research interest is the development of laser techniques and their application to different mechanical problems. She worked on holographic interferometry as a fluid velocimetry technique and combined it with particle image velocimetry for three component velocity measurements in a fluid plane. She has also worked on digital speckle pattern interferometry as a solid deformation technique.

Ana Andres-Arroyo received a bachelor of physics at the University of Zaragoza. She spent one year on exchange during undergraduate studies at the University of New South Wales. She is currently undertaking a PhD in physics with Dr. Peter Reece in the optoelectronics area at the University of New South Wales. Her field of study is optical trapping and characterization of metallic nanoparticles.

M. Pilar Arroyo is a full professor of applied physics. Her research interest focuses on the development of experimental optical techniques for mechanical measurements. She has published key papers on particle image velocimetry (PIV), holographic interferometry, digital speckle pattern interferometry (DSPI), and digital holography. These techniques have been applied to hemodynamic flows in aneurysm models and in veins with antithrombotic filters.

Virginia R. Palero is associated professor of applied physics at the University of Zaragoza since 2002. Since 2006, she has been the Spanish representative at the Management Committee of two subsequent COST actions related to the physics of droplets. Her research interests include digital holography, droplets mechanics, and biological flows.

Julia Lobera is lecturer at the CUD (Centro Universitario de la Defensa) and an associated member of the TOL research group of the Aragón Institute of Engineering Research (I3A). Her main research interest is in optical metrology, where she has coauthored key papers in holographic particle image velocimetry (HPIV) and in digital image plane holography. She is currently working toward the implementation of optical diffraction tomography in HPIV and on the application of several holographic methods to the flow characterization in aneurism models and droplets.

Luis A. Angurel is full professor at the University of Zaragoza. He is a member of the Aragon Materials Science Institute, a joint institute between the Spanish Research Council and the University of Zaragoza. His main research topics are the fabrication and characterization of superconducting materials for large-scale electrical applications and the use of laser technologies in materials processing. He has been working in the introduction of optical techniques in the characterization of high temperature superconductors thermal stability and environmental degradation processes.